

# Integration Matters for Learning PDEs with Backwards SDEs

Sungje Park<sup>1</sup> and Stephen Tu<sup>2</sup>

<sup>1</sup>Department of Aerospace Engineering, Embry-Riddle Aeronautical University

<sup>2</sup>Department of Electrical and Computer Engineering, University of Southern California

May 5, 2025

## Abstract

Backward stochastic differential equation (BSDE)-based deep learning methods provide an alternative to Physics-Informed Neural Networks (PINNs) for solving high-dimensional partial differential equations (PDEs), offering algorithmic advantages in settings such as stochastic optimal control, where the PDEs of interest are tied to an underlying dynamical system. However, existing BSDE-based solvers have empirically been shown to underperform relative to PINNs in the literature. In this paper, we identify the root cause of this performance gap as a discretization bias introduced by the standard Euler-Maruyama (EM) integration scheme applied to short-horizon self-consistency BSDE losses, which shifts the optimization landscape off target. We find that this bias cannot be satisfactorily addressed through finer step sizes or longer self-consistency horizons. To properly handle this issue, we propose a Stratonovich-based BSDE formulation, which we implement with stochastic Heun integration. We show that our proposed approach completely eliminates the bias issues faced by EM integration. Furthermore, our empirical results show that our Heun-based BSDE method consistently outperforms EM-based variants and achieves competitive results with PINNs across multiple high-dimensional benchmarks. Our findings highlight the critical role of integration schemes in BSDE-based PDE solvers, an algorithmic detail that has received little attention thus far in the literature.

## 1 Introduction

Numerical solutions to partial differential equations (PDEs) are foundational to modeling problems across a diverse set of fields in science and engineering. However, due to the curse of dimensionality of traditional numerical methods, application of classic solvers to high dimensional PDEs is computationally intractable. In recent years, motivated by the success of deep learning methods in machine learning, both Physics-Informed Neural Networks (PINNs) [1, 2] and backward stochastic differential equation (BSDE) based methods [3–5] have emerged as promising scalable alternatives to classic mesh-based techniques for solving PDEs. At a high level, these approaches utilize neural networks and gradient-based optimization to efficiently parameterize and learn solutions to high-dimensional PDEs.

Despite the widespread popularity of PINNs methods, in this paper we focus on the use of BSDE-based methods for solving high-dimensional PDEs. The key difference between PINNs and BSDE methods is that while PINNs minimize the PDE residual directly on randomly sampled collocation points, BSDE methods reformulate PDEs as forward-backward SDEs (FBSDEs) and simulate the resulting stochastic processes to minimize the discrepancy between predicted and terminal conditions at the end of the forward SDE trajectory [3] or across an intermediate time-horizon via *self-consistency* losses [4, 5]. BSDE methods are especially well-suited for high-dimensional problems where there is underlying dynamics—such as in stochastic optimal control or quantitative finance—as the crux of these methods involving sampling over stochastic trajectories rather than over bounded spatial domains. Furthermore, BSDE methods offers a significant advantage in problems where the governing equations of the PDE are unknown and can only be accessed

through simulation [6], as in model-free optimal control/reinforcement learning problems. In contrast, PINNs methods require explicit knowledge of the PDE equations, which may be either be impractical to obtain for various tasks or require a separate model learning step within the training pipeline.

Surprisingly, despite the aforementioned benefits of BSDE methods compared with PINNs, a thorough comparison between the two techniques remains largely absent from the literature. One notable exception is recent work by [5] which finds that on several benchmark problems, PDE solutions found by BSDE-based approaches significantly underperform the corresponding PINNs solutions. To address this gap, they propose a hybrid *interpolating* loss between the PINNs and BSDE losses. While promising, their result has two key disadvantages. First, the underlying cause of the performance gap between BSDE and PINNs methods is not elucidated, and it is unclear what mechanisms are at play that allow their interpolation loss to yield better performance. Second, their method introduces a new hyperparameter (the horizon-length which controls the level of interpolation) which must be tuned for optimal performance, adding more complexity to the already delicate training process for PINNs [2].

In this work, we identify the key source of the performance gap between BSDE and PINNs methods to be the standard Euler-Maruyama (EM) scheme used to integrate the backwards SDE. Although simple to implement, we show that the EM scheme introduces a significant discretization bias in *short-horizon* BSDE losses, resulting in a discrepancy between the optimization objective and the true solution. We furthermore show that the EM discretization bias can only be made arbitrarily small by using *long-horizon* BSDE losses, which we show both theoretically and empirically comes at a significant cost in performance. Within the context of our analysis, we understand the interpolating loss of [5] as attempting to find (via hyperparameter tuning) the optimal BSDE horizon length subject to the use of EM integration.

As an alternative, we propose interpreting both the forward and backwards SDEs as Stratonovich SDEs, as opposed to Itô SDEs, and utilizing the stochastic Heun intergration scheme for numerical integration. We prove that the use of the stochastic Heun method completely eliminates the non-vanishing bias issues which occur in the EM formulation for short-horizon BSDE losses. This removes all performance tradeoffs in the horizon-length, allowing us to utilize single-step self-consistency losses. The result is a practical BSDE-based algorithm that is competitive with PINNs methods without the need for interpolating losses.

**Contributions.** We make the following concrete contribution in this work:

- (a) We show (Section 4.1) that the integration method is a crucial design decision when implementing short-horizon self-consistency BSDE losses: the default EM algorithm introduces *bias* to the loss which cannot be controlled by sufficient discretization. Fortunately, we also show (Section 4.2) that using a higher order *Stratonovich* integrator—specifically the stochastic Heun algorithm [7]—removes this integration bias.
- (b) We show (Section 5) that while these integration issues can be mitigated in the EM integration scheme by utilizing longer horizon self-consistency losses, doing so comes with trade-offs in the optimization loss landscape.
- (c) We conduct a thorough empirical study (Section 6) of these issues on several high dimensional PDEs, and illustrate the following key findings: (1) EM-based BSDE methods consistently underperforms PINNs, even in high dimensional cases. (2) Heun integration closes the gap between BSDE and PINNs losses. (3) While longer horizon self-consistency in EM-BSDE losses improves results, it fails to match the performance of Heun-BSDE, even with finer discretizations.

Through the theoretical and empirical analysis of numerical discretization in BSDE-based deep PDE solvers, we demonstrate the critical role of integrator choice in BSDE solver performance. Surprisingly, prior to our work this detail has received little attention in the literature. We hope that our work inspires further algorithmic and implementation level improvements for BSDE solvers.

## 2 Related Work

In recent years, PINNs [1, 8–12] has emerged as a popular method for solving high dimensional PDEs. PINNs methods parameterize the PDE solution as a neural network and directly minimize the PDE residual as a loss function, provides a mesh-free method that can easily incorporate complex boundary conditions and empirical data. However, the PINNs approach remains an incomplete solution and still suffers from many issues including optimization challenges [13–15], despite a concerted effort to remedy these difficulties [2, 13, 14, 16–20]. Hence, the application of PINNs as a reliable, general purpose solver for complex high-dimensional PDEs has yet to be realized.

On the other hand, a complementary line of work proposes methods based on BSDEs to solve high-dimensional PDEs [3–5, 21–25]. These approaches reformulate PDEs as forward-backward SDEs to derive a trajectory-based loss. While the original deep BSDE methods [3, 21, 22] learn separate neural networks to predict both the value and gradient at each discrete time-step, follow up work [4, 5] uses *self-consistency*, i.e., the residual of stochastic integration along BSDE trajectories, to form a loss. In this work, we exclusive focus on self-consistency BSDE losses, as they generalize the original method while allowing for a single network to parameterization the PDE solution for all space and time, similarly to PINNs. Similar self-consistency losses have also been recently utilized to learn solutions to Fokker-Planck PDEs [26–28].

The main purpose of our work is to understand the performance differences between PINNs and BSDE methods on high-dimensional PDEs. The most relevant work to ours is that of [5], which to the best of our knowledge is the only work in the literature which directly compares PINNs and BSDE methods in a head-to-head evaluation. As discussed in Section 1, our work shows that the gap in performance between PINNs and BSDE methods observed in [5] is due to the choice of stochastic integration. Again, to the best of our knowledge, the role of the integration scheme in BSDE methods for solving PDEs has not been considered before in the literature.

## 3 Background and Contributions

We consider learning approximate solutions to the following family of non-linear boundary value PDEs

$$R[u](x, t) := \partial_t u(x, t) + \frac{1}{2} \text{tr}(H(x, t) \cdot \nabla^2 u(x, t)) + \langle f(x, t), \nabla u(x, t) \rangle - h(x, t, u(x, t), \nabla u(x, t)) = 0, \quad (3.1)$$

over domain  $x \in \Omega \subseteq \mathbb{R}^d$ ,  $t \in [0, T]$  with boundary conditions

$$u(x, T) = \phi(x) \quad \forall x \in \Omega, \quad (3.2)$$

$$u(x, t) = \phi_b(x, t) \quad \forall x \in \partial\Omega, t \in [0, T]. \quad (3.3)$$

Here,  $u : \Omega \times [0, T] \mapsto \mathbb{R}$  is a candidate PDE solution,  $f : \Omega \times [0, T] \mapsto \mathbb{R}^d$  is a vector-field,  $h : \Omega \times [0, T] \times \mathbb{R} \times \mathbb{R}^d \mapsto \mathbb{R}$  captures the non-linear terms,  $H(x, t) = g(x, t)g(x, t)^\top \in \mathbb{R}^{d \times d}$  is a positive definite matrix-valued function,  $\phi : \Omega \times [0, T]$  and  $\phi_b : \partial\Omega \times [0, T]$  are boundary conditions, and both  $\nabla$  and  $\nabla^2$  denote spatial gradients and Hessians, respectively. For expositional clarity in this section, we will assume that  $\Omega = \mathbb{R}^d$  and hence drop the second boundary condition (3.3), noting that all subsequent arguments can be extended in a straightforward manner for bounded domains  $\Omega$ .

**Physics-Informed Neural Networks (PINNs).** Under the assumption of knowledge of the operator  $R[u]$  and the boundary condition  $\phi$ , the standard PINNs methodology [1, 8–11] for solving (3.1) works by parameterizing the solution  $u(x, t)$  in a function class  $\mathcal{U} := \{u_\theta(x, t) \mid \theta \in \Theta\}$  (e.g.,  $\theta$  represents the weights of a neural network), and minimizing the PINNs loss over this function class  $\mathcal{U}$ :<sup>1</sup>

$$L_{\text{PINNs}}(\theta; \lambda) := \mathbb{E}_{(x, t) \sim \mu}[(R[u_\theta](x, t))^2] + \lambda \cdot \mathbb{E}_{x \sim \mu'}[(u_\theta(x, T) - \phi(x))^2], \quad (3.4)$$

---

<sup>1</sup>We leave consideration of the PINNs loss with non-square losses (e.g., [18]) to future work.

where  $\mu$  is a measure over  $\Omega \times [0, T]$  and  $\mu'$  is a measure over  $\Omega$ . The choice of measures  $\mu, \mu'$ , in addition to the relative weight  $\lambda$  are hyperparameters which must be carefully selected by the user. To simplify exposition further, we will assume that each  $u_\theta(x, t) \in \mathcal{U}$  satisfies  $u(\cdot, T) = \phi$  (e.g., as is done in practice in [29, 30]), so that the boundary condition does not need to be added to the loss, and hence the PINNs loss simplifies further to  $L_{\text{PINNs}}(\theta) = \mathbb{E}_{(x, t) \sim \mu}[(R[u_\theta](x, t))^2]$ .

**Backwards SDEs and Self-Consistency Losses.** While the PINNs loss has received much attention in the past few years, a separate line of work has advocated for an alternative approach to solving PDEs based on backwards SDEs [3, 4, 21–23]. The key idea is that if we consider the following *forward (Itô) SDE*:

$$dX_t = f(X_t, t)dt + g(X_t, t)dB_t, \quad X_0 = x_0, \quad (3.5)$$

where  $(B_t)_{t \geq 0}$  is standard Brownian motion in  $\mathbb{R}^d$ , then the following *backwards (Itô) SDE*

$$dY_t = h(X_t, t, Y_t, Z_t)dt + Z_t^\top g(X_t, t)dB_t, \quad Y_T = \phi(X_T), \quad (3.6)$$

is solved by setting  $Y_t = u(X_t, t)$  and  $Z_t = \nabla u(X_t, t)$ , where  $u$  solves the PDE (3.1); this equivalence is readily shown with Itô's lemma. This relationship between the forward and backwards SDE has motivated several different types of BSDE loss functions for solving (3.1). The original BSDE losses [3, 21] learn  $N$  models to predict both  $Y_t$  and  $Z_t$  at  $N$  discretization points. These BSDE losses further require retraining these models for every new initiation condition of  $X_0$ , but this requirement is removed in follow-up works on backwards recursion BSDE variants [22, 23].

In this work, we focus instead on BSDE losses based on *self-consistency* [4, 5], which uses the residual of stochastic integration along the BSDE trajectories to form a loss. Self-consistency losses are substantially more practical than other variants as only one network is required and the weights can be shared across time. The most general form of self-consistency BSDE losses is due to [5], who define the following:

$$L_{\text{BSDE}}(\theta) := \mathbb{E}_{\substack{x_0 \sim \mu_0, \\ (t_s, t_f) \sim \rho, B_t}} \frac{1}{\Delta_t^2} \left( u_\theta(X_{t_f}, t_f) - u_\theta(X_{t_s}, t_s) - \int_{t_s}^{t_f} h_\theta(X_t, t)dt - \int_{t_s}^{t_f} \nabla u_\theta(X_t, t)^\top g(X_t, t)dB_t \right)^2, \quad (3.7)$$

where  $\rho$  is a distribution over  $[0, T] \times [0, T]$  such that  $(t_s, t_f) \sim \rho$  satisfies  $0 \leq t_s < t_f \leq T$ , and  $\Delta_t := t_f - t_s$ . Note that in Equation (3.7), we use the shorthand  $h_\theta(x, t) := h(x, t, u_\theta(x, t), \nabla u_\theta(x, t))$ . An important special case of (3.7) is what we refer to as a *one-step* or *single-step* self-consistency loss. Here, we choose a positive integer  $N \in \mathbb{N}_+$ , select a step-size  $\tau := T/N$ , and choose our time-pair distribution  $\rho$  of the form  $t_s \sim \text{Unif}(\{t_k\}_{k=0}^{N-1})$  and  $t_f = t_s + \tau$ , with  $t_k := k\tau$ . In this case, (3.7) simplifies to:

$$L_{\text{BSDE}, \tau}(\theta) := \mathbb{E}_{x_0 \sim \mu_0, B_t} \frac{1}{N\tau^2} \sum_{k=0}^{N-1} \left( u_\theta(X_{t_{k+1}}, t_{k+1}) - u_\theta(X_{t_k}, t_k) - \int_{t_k}^{t_{k+1}} h_\theta(X_t, t)dt - \int_{t_k}^{t_{k+1}} \nabla u_\theta(X_t, t)^\top g(X_t, t)dB_t \right)^2, \quad (3.8)$$

recovering the self-consistent BSDE variant from [4], also discussed in [31, 32].

**Stochastic Integration.** Unlike the PINNs loss (3.4), the BSDE losses (3.7) and (3.8) cannot be directly implemented as written, and instead the stochastic integration which appears must be discretized with an appropriate stochastic integrator. The standard choice is to use the classic Euler-Maruyama (EM) method, selecting a step size  $\tau > 0$ , and jointly integrating the forward and backwards SDEs as follows:

$$\hat{X}_{k+1} = \hat{X}_k + f(\hat{X}_k, t_k)\tau + \sqrt{\tau}g(\hat{X}_k, t_k)w_k, \quad w_k \sim \mathcal{N}(0, I_d), \quad \hat{X}_0 = x_0, \quad (3.9)$$

$$\hat{Y}_{k+1}^\theta = \hat{Y}_k^\theta + h_\theta(\hat{X}_k, t_k)\tau + \sqrt{\tau}\nabla u_\theta(\hat{X}_k, t_k)^\top g(\hat{X}_k, t_k)w_k, \quad \hat{Y}_0^\theta = u_\theta(x_0, 0). \quad (3.10)$$

Here, note that the noises  $w_k$  are *coupled* between  $\hat{X}_k$  and  $\hat{Y}_k^\theta$ . With this discretization in hand, the EM versions of  $L_{\text{BSDE}}$  and  $L_{\text{BSDE},\tau}$  are respectively,

$$L_{\text{EM}}(\theta) := \mathbb{E}_{\substack{x_0 \sim \mu_0 \\ (k_1, k_2) \sim \rho, w_k}} \frac{1}{\Delta_t^2} \left( u_\theta(\hat{X}_{k_2}, t_{k_2}) - u_\theta(\hat{X}_{k_1}, t_{k_1}) - (\hat{Y}_{k_2}^\theta - \hat{Y}_{k_1}^\theta) \right)^2, \quad (3.11)$$

$$L_{\text{EM},\tau}(\theta) := \mathbb{E}_{x_0 \sim \mu_0, w_k} \frac{1}{N\tau^2} \sum_{k=0}^{N-1} \left( u_\theta(\hat{X}_{k+1}, t_{k+1}) - u_\theta(\hat{X}_k, t_k) - (\hat{Y}_{k+1}^\theta - \hat{Y}_k^\theta) \right)^2. \quad (3.12)$$

Here for  $L_{\text{EM}}$  we assumed for simplicity that the times returned by the time-pair distribution  $\rho$  align exactly with the discretization times  $\{t_k\}$ , and overland notation to reflect this simplification.

## 4 Analysis of One-Step Self-Consistency Losses

In this section we conduct an analysis of the one-step self-consistency BSDE loss (3.8), in particular its Euler-Maruyama variant versus Stratonovich variant.

**The Hölder space of  $C^{k,1}$  functions.** Let  $f : M \mapsto M'$ , where both  $M, M'$  are subsets of Euclidean space (with possibly different dimension). We say that  $f$  is  $C^{k,1}(M, M')$  if  $f$  is  $k$ -times continuously differentiable on  $M$ , and the  $k$ -th derivative of  $f$  is Lipschitz continuous, i.e., there exists a finite  $L > 0$  such that  $\|D^k f(x) - D^k f(y)\| \leq L\|x - y\|$  for all  $x, y \in M$ . When both  $M, M'$  are clear given the context, we will utilize the shorthand  $C^{k,1}$ .

### 4.1 Analysis of Euler-Maruyama for BSDE

We will first illustrate the bias present in the EM scheme. To do this, we define the *one-step* EM loss at resolution  $\tau$  for a fixed  $(x, t) \in \mathbb{R}^d \times [0, T]$  as:

$$\begin{aligned} \ell_{\text{EM},\tau}(\theta, x, t) &:= \mathbb{E}_w \left( u_\theta(\hat{x}_{t+\tau}, t + \tau) - u_\theta(x, t) - h_\theta(x, t)\tau - \sqrt{\tau} \langle \nabla u_\theta(x, t), g(x, t)w \rangle \right)^2, \\ \hat{x}_{t+\tau} &:= x + f(x, t)\tau + \sqrt{\tau}g(x, t)w, \quad w \sim \mathcal{N}(0, I_d). \end{aligned} \quad (4.1)$$

Observe that the one-step loss (4.1) is precisely the loss in the summand in (3.12) once we condition on  $X_k$ :

$$L_{\text{EM},\tau}(\theta) = \frac{1}{N\tau^2} \sum_{k=0}^{N-1} \mathbb{E}_{\hat{X}_k} [\ell_{\text{EM},\tau}(\theta, \hat{X}_k, t_k)]. \quad (4.2)$$

Our first result shows that the dominant error term (in  $\tau$ ) of the (4.1) loss suffers from an additive bias term to the PDE residual that is introduced as a result of the EM integration scheme.

**Lemma 4.1.** *Suppose that  $u_\theta$  is  $C^{2,1}$ . We have that*

$$\lim_{\tau \rightarrow 0^+} \tau^{-2} \cdot \ell_{\text{EM},\tau}(\theta, x, t) = (R[u_\theta](x, t))^2 + \frac{1}{2} \text{tr} \left[ (H(x, t) \cdot \nabla^2 u_\theta(x, t))^2 \right]. \quad (4.3)$$

Before we prove Lemma 4.1, we recall a standard formula for the variance of Gaussian quadratic forms.

**Proposition 4.2.** *Let  $Q$  be a  $d \times d$  symmetric matrix and  $w \sim \mathcal{N}(0, I_d)$ . Then,*

$$\mathbb{E}_w (\text{tr}(Q) - w^\top Q w)^2 = 2\|Q\|_F^2.$$

*Proof.* We have that  $\mathbb{E}_w (\text{tr}(Q) - w^\top Q w)^2 = \mathbb{E}_w (w^\top Q w)^2 - \text{tr}(Q)^2$ . From [cf. 33, Lemma 2.2] we obtain the identity  $\mathbb{E}_w (w^\top Q w)^2 = 2\text{tr}(Q^2) + \text{tr}(Q)^2$ , which concludes the proof.  $\square$

With Proposition 4.2 in place, we now turn to the proof of Lemma 4.1.

*Proof of Lemma 4.1.* We first introduce two pieces of notation:  $O(\cdot)$  and  $O^*(\cdot)$ . The former  $O(\cdot)$  hides constants that depend arbitrarily on  $\theta, x, t$ , whereas the latter  $O^*(\cdot)$  in addition also hides constants that depend *polynomially* on  $\|w\|$ . The latter polynomial dependence is important when we take expectations of powers of  $O^*(\cdot)$  terms, since  $\mathbb{E}\|w\|^p$  is finite for any finite  $p \in \mathbb{N}$ .

Since  $u \in C^{2,1}$ , setting  $\bar{\Delta} := (\hat{x}_{t+\tau} - x, \tau) \in \mathbb{R}^{d+1}$  and suppress dependency on  $\theta$  in our notation, a second-order Taylor expansion yields:

$$\begin{aligned} u(\hat{x}_{t+\tau}, t + \tau) - u(x, t) &= Du(x, t)\bar{\Delta} + \frac{1}{2}\bar{\Delta}^\top D^2u(x, t)\bar{\Delta} + O(\|\bar{\Delta}\|^3), \\ Du(x, t)\bar{\Delta} &= \langle \nabla u(x, t), \hat{x}_{t+\tau} - x \rangle + \partial_t u(x, t)\tau, \\ \frac{1}{2}\bar{\Delta}^\top D^2u(x, t)\bar{\Delta} &= \frac{1}{2} \left( (\hat{x}_{t+\tau} - x)^\top \nabla^2 u(x, t) (\hat{x}_{t+\tau} - x) + 2\tau \langle \partial_t \nabla u(x, t), \hat{x}_{t+\tau} - x \rangle + \tau^2 \partial_t^2 u(x, t) \right), \end{aligned}$$

Plugging in  $\hat{x}_{t+\tau} - x = f(x, t)\tau + \sqrt{\tau}g(x, t)w$ , we obtain:

$$\begin{aligned} &(u(\hat{x}_{t+\tau}, t + \tau) - u(x, t)) - (h(x, t)\tau - \sqrt{\tau}\langle \nabla u(x, t), g(x, t)w \rangle) \\ &= \tau \left[ \langle \nabla u(x, t), f(x, t) \rangle + \partial_t u(x, t) - h(x, t) + \frac{1}{2}w^\top g(x, t)^\top \nabla^2 u(x, t)g(x, t)w \right] + O^*(\tau^{3/2}) \\ &= \tau \left[ R[u](x, t) - \frac{1}{2} \text{tr}(H(x, t) \cdot \nabla^2 u(x, t)) + \frac{1}{2}w^\top g(x, t)^\top \nabla^2 u(x, t)g(x, t)w \right] + O^*(\tau^{3/2}), \end{aligned}$$

where in the last equality we used the definition of the PDE residual from (3.1). Hence,

$$\begin{aligned} \ell_{\text{EM}, \tau}(x, t) &= \mathbb{E}_w(u(\hat{x}_{t+\tau}, t + \tau) - u(x, t)) - (h(x, t)\tau - \sqrt{\tau}\langle \nabla u(x, t), g(x, t)w \rangle)^2 \\ &= \tau^2 \cdot \mathbb{E}_w \left( R[u](x, t) - \frac{1}{2} \text{tr}(H(x, t) \cdot \nabla^2 u(x, t)) + \frac{1}{2}w^\top g(x, t)^\top \nabla^2 u(x, t)g(x, t)w \right)^2 + O(\tau^{5/2}) \\ &= \tau^2 \left( (R[u](x, t))^2 + \frac{1}{4}\mathbb{E}_w \left( \text{tr}(H(x, t) \cdot \nabla^2 u(x, t)) - w^\top g(x, t)^\top \nabla^2 u(x, t)g(x, t)w \right)^2 \right) + O(\tau^{5/2}) \\ &= \tau^2 \left( (R[u](x, t))^2 + \frac{1}{2} \text{tr}((H(x, t) \cdot \nabla^2 u(x, t))^2) \right) + O(\tau^{5/2}), \end{aligned}$$

where the final equality follows from Proposition 4.2. The claim now follows.  $\square$

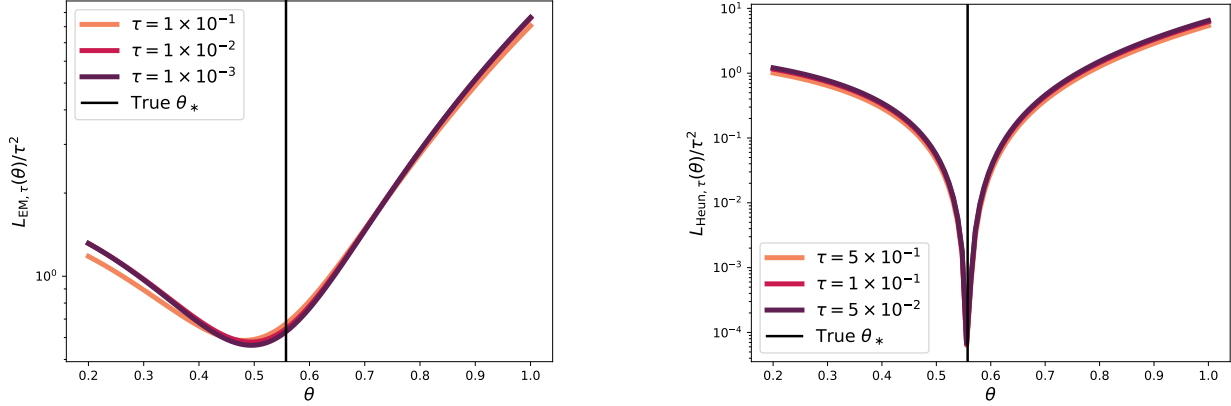
While the proof of Lemma 4.1 is relatively straightforward, its implication is non-trivial. Let us further assume that the standard regularity conditions are in place for the forward SDE (3.5) such that the Euler-Maruyama scheme satisfies order 1/2 strong convergence [34], i.e.,

$$\left( \mathbb{E} \left[ \max_{k \in \{0, \dots, N-1\}} \|\hat{X}_k - X_{t_k}\|^2 \right] \right)^{1/2} \leq C\tau^{1/2}, \quad (4.4)$$

where  $C$  is a constant that is independent of  $\tau$  (but may depend on  $T$  and properties of the forward SDE). By combining (4.4) with some standard regularity assumptions on  $R[u_\theta]$ ,  $H$ , and  $u_\theta$  combined with the approximation properties of a Riemann sum:

$$\begin{aligned} L_{\text{EM}, \tau}(\theta) &= \frac{1}{N} \sum_{k=0}^{N-1} \mathbb{E} \left( (R[u_\theta](\hat{X}_k, t_k))^2 + \frac{1}{2} \text{tr}((H(\hat{X}_k, t_k) \cdot \nabla^2 u_\theta(\hat{X}_k, t_k))^2) \right) + O(\tau^{1/2}) \\ &= \frac{1}{T} \int_0^T \mathbb{E} \left( (R[u_\theta](X_t, t))^2 + \frac{1}{2} \text{tr}((H(X_t, t) \cdot \nabla^2 u_\theta(X_t, t))^2) \right) dt + O(\tau^{1/2}). \end{aligned} \quad (4.5)$$

The expression (4.5) implies that even if the function class  $\mathcal{U}$  is expressive enough to contain a true PDE solution  $u_{\theta_*}$  to (3.1) which satisfies  $R[u_{\theta_*}] = 0$ , in general  $L_{\text{EM}, \tau}(\theta_*) > \inf_{u_\theta \in \mathcal{U}} L_{\text{EM}, \tau}(\theta)$ , and hence optimizing  $L_{\text{EM}, \tau}(\theta)$  can lead to sub-optimal solutions *even in the limit of infinite simulated trajectories*. Furthermore, this bias *cannot* be resolved by simply reducing the step size  $\tau$ , since the PDE residual term and the bias term are both the same order in terms of  $\tau$ . We illustrate this phenomenon with a one-dimensional example in Figure 1a.



(a) Plot of  $L_{\text{EM},\tau}(\theta)$  at  $\tau \in \{10^{-1}, 10^{-2}, 10^{-3}\}$  levels of discretization.

(b) Plot of  $L_{\text{Heun},\tau}(\theta)$  at  $\tau \in \{5 \times 10^{-1}, 10^{-1}, 5 \times 10^{-2}\}$  levels of discretization.

**Figure 1:** A plot of both  $L_{\text{EM},\tau}(\theta)$  and  $L_{\text{Heun},\tau}(\theta)$  at various levels of discretization step size  $\tau$ . The PDE here is a one dimensional linear quadratic regular (LQR) Hamilton-Jacobi-Bellman equation, where the  $\theta$  parameterizes a quadratic value function.

## 4.2 Stratonovich BSDEs and Stochastic Heun Integration

Our next step is to derive a new BSDE loss based on Heun integration. Our starting point is to interpret the forward SDE as a Stratonovich SDE (in contrast to (3.5)):

$$dX_t^\bullet = f(X_t^\bullet, t)dt + g(X_t^\bullet, t) \circ dB_t, \quad X_0^\bullet = x_0. \quad (4.6)$$

In Equation (4.6), we use the  $\circ$  marker to denote that the forward SDE is to be interpreted in the sense of Stratonovich. For the special case where  $g(x, t)$  is a constant, then there is no difference between (4.6) and (3.5). Now, for any  $u$  that satisfies the PDE (3.1), using the ordinary chain rule:

$$\begin{aligned} du(X_t^\bullet, t) &= [\langle \nabla u(X_t^\bullet, t), f(X_t^\bullet, t) \rangle + \partial_t u(X_t^\bullet, t)] dt + \nabla u(X_t^\bullet, t)^\top g(X_t^\bullet, t) \circ dB_t \\ &= \left[ h(X_t^\bullet, t, u(X_t^\bullet, t), \nabla u(X_t^\bullet, t)) - \frac{1}{2} \text{tr}(H(X_t^\bullet, t) \nabla^2 u(X_t^\bullet, t)) \right] dt + \nabla u(X_t^\bullet, t)^\top g(X_t^\bullet, t) \circ dB_t. \end{aligned} \quad (4.7)$$

This motivates the following Stratonovich BSDE loss and its one step variant:

$$\begin{aligned} L_{\text{S-BSDE}}(\theta) &:= \mathbb{E}_{\substack{x_0 \sim \mu_0, \\ (t_s, t_f) \sim \rho, B_t}} \frac{1}{\Delta_t^2} \left( u_\theta(X_{t_f}^\bullet, t_f) - u_\theta(X_{t_s}^\bullet, t_s) - \int_{t_s}^{t_f} \left[ h_\theta(X_t^\bullet, t) - \frac{1}{2} \text{tr}(H(X_t^\bullet, t) \nabla^2 u_\theta(X_t^\bullet, t)) \right] dt \right. \\ &\quad \left. - \int_{t_s}^{t_f} \nabla u_\theta(X_t^\bullet, t)^\top g(X_t^\bullet, t) \circ dB_t \right)^2, \end{aligned} \quad (4.8)$$

$$\begin{aligned} L_{\text{S-BSDE},\tau}(\theta) &:= \mathbb{E}_{x_0 \sim \mu_0, B_t} \frac{1}{N\tau^2} \sum_{k=0}^{N-1} \left( u_\theta(X_{t_{k+1}}^\bullet, t_{k+1}) - u_\theta(X_{t_k}^\bullet, t_k) \right. \\ &\quad \left. - \int_{t_k}^{t_{k+1}} \left[ h_\theta(X_t^\bullet, t) - \frac{1}{2} \text{tr}(H(X_t^\bullet, t) \nabla^2 u_\theta(X_t^\bullet, t)) \right] dt - \int_{t_k}^{t_{k+1}} \nabla u_\theta(X_t^\bullet, t)^\top g(X_t^\bullet, t) \circ dB_t \right)^2, \end{aligned} \quad (4.9)$$

with  $X_t^\bullet$  following the forward SDE (4.6). As both (4.8) and (4.9) utilize Stratonovich integration, the Euler-Maruyama scheme cannot be used for integration, as it converges to the Itô solution. Hence, we will consider the stochastic Heun integrator [7, 34] which has the favorable property of converging to the Stratonovich solution. We proceed first by defining the augmented forward and backwards SDE:

$$d \begin{bmatrix} X_t^\bullet \\ Y_t^{\bullet,\theta} \end{bmatrix} = \begin{bmatrix} f(X_t^\bullet, t) \\ h_\theta(X_t^\bullet, t) - \frac{1}{2} \text{tr}(H(X_t^\bullet, t) \nabla^2 u_\theta(X_t^\bullet, t)) \end{bmatrix} dt + \begin{bmatrix} g(X_t^\bullet, t) \\ \nabla u_\theta(X_t^\bullet, t)^\top g(X_t^\bullet, t) \end{bmatrix} \circ dB_t, \quad \begin{bmatrix} X_0 \\ Y_0^{\bullet,\theta} \end{bmatrix} = \begin{bmatrix} x_0 \\ u_\theta(x_0, 0) \end{bmatrix},$$

$$=: F_\theta(Z_t^{\bullet,\theta}, t) dt + G_\theta(Z_t^{\bullet,\theta}, t) \circ dB_t, \quad Z_t^{\bullet,\theta} := (X_t^\bullet, Y_t^{\bullet,\theta}).$$

We then discretize the augmented SDE as follows using the stochastic Heun scheme:

$$\bar{Z}_{k+1}^{\bullet,\theta} = \hat{Z}_k^{\bullet,\theta} + F_\theta(\hat{Z}_k^{\bullet,\theta}, t_k) \tau + G_\theta(\hat{Z}_k^{\bullet,\theta}, t_k) \sqrt{\tau} w_k, \quad \hat{Z}_0^{\bullet,\theta} = (x_0, u_\theta(x_0, 0)), \quad (4.10)$$

$$\hat{Z}_{k+1}^{\bullet,\theta} = \hat{Z}_k^{\bullet,\theta} + \frac{1}{2} \left( F_\theta(\hat{Z}_k^{\bullet,\theta}, t_k) + F_\theta(\bar{Z}_{k+1}^{\bullet,\theta}, t_{k+1}) \right) \tau + \frac{1}{2} \left( G_\theta(\hat{Z}_k^{\bullet,\theta}, t_k) + G_\theta(\bar{Z}_{k+1}^{\bullet,\theta}, t_{k+1}) \right) \sqrt{\tau} w_k, \quad (4.11)$$

with  $w_k \sim \mathcal{N}(0, I_d)$ . Now, similar to how we proceeded for EM, we can define two Heun losses as:

$$L_{\text{Heun}}(\theta) := \mathbb{E}_{\substack{x_0 \sim \mu_0 \\ (k_1, k_2) \sim \rho, w_k}} \frac{1}{\Delta_t^2} \left( u_\theta(\hat{X}_{k_2}^\bullet, t_{k_2}) - u_\theta(\hat{X}_{k_1}^\bullet, t_{k_1}) - (\hat{Y}_{k_2}^{\bullet,\theta} - \hat{Y}_{k_1}^{\bullet,\theta}) \right)^2, \quad (4.12)$$

$$L_{\text{Heun},\tau}(\theta) := \mathbb{E}_{x_0 \sim \mu_0, w_k} \frac{1}{N\tau^2} \sum_{k=0}^{N-1} \left( u_\theta(\hat{X}_{k+1}^\bullet, t_{k+1}) - u_\theta(\hat{X}_k^\bullet, t_k) - (\hat{Y}_{k+1}^{\bullet,\theta} - \hat{Y}_k^{\bullet,\theta}) \right)^2, \quad (4.13)$$

where the  $\hat{Z}_k^{\bullet,\theta} = (\hat{X}_k^\bullet, \hat{Y}_k^{\bullet,\theta})$  iterates arise from the stochastic Heun scheme (4.10), (4.11). We now show that the use of Heun in (4.13) avoids the undesirable bias term which appears when using Euler-Maruyama discretization (cf. Section 4.1, (3.12)). To do this, we define the one-step Heun self-consistency loss as:

$$\ell_{\text{Heun},\tau}(\theta, x, t) := \mathbb{E}_w (u_\theta(\hat{x}_{t+\tau}, t + \tau) - \hat{y}_{t+\tau}^\theta)^2, \quad (4.14)$$

$$\bar{z}_{t+\tau}^\theta = z_t^\theta + F_\theta(z_t^\theta, t) \tau + G_\theta(z_t^\theta, t) \sqrt{\tau} w, \quad (4.15)$$

$$\hat{z}_{t+\tau}^\theta = z_t^\theta + \frac{1}{2} (F_\theta(z_t^\theta, t) + F_\theta(\bar{z}_{t+\tau}^\theta, t + \tau)) \tau + \frac{1}{2} (G_\theta(z_t^\theta, t) + G_\theta(\bar{z}_{t+\tau}^\theta, t + \tau)) \sqrt{\tau} w, \quad (4.16)$$

$$\hat{z}_{t+\tau}^\theta = (\hat{x}_{t+\tau}, \hat{y}_{t+\tau}^\theta), \quad z_t^\theta = (x, u_\theta(x, t)). \quad (4.17)$$

Again similar to (4.2), we have the following identity  $L_{\text{Heun},\tau}(\theta) = \frac{1}{N\tau^2} \sum_{k=0}^{N-1} \mathbb{E}_{\hat{X}_k^\bullet} [\ell_{\text{Heun},\tau}(\theta, \hat{X}_k^\bullet, t_k)]$ . Our next result illustrates that this one-step Heun loss avoids the issues identified with EM in Lemma 4.1.

**Lemma 4.3.** *Suppose that  $f$ ,  $g$ , and  $h_\theta$  are all in  $C^{1,1}$ , and  $u_\theta$  is in  $C^{2,1} \cap C^{3,1}$ . We have that*

$$\lim_{\tau \rightarrow 0^+} \tau^{-2} \cdot \ell_{\text{Heun},\tau}(\theta, x, t) = (R[u_\theta](x, t))^2. \quad (4.18)$$

*Proof.* For what follows, we drop the dependency in the notation on  $\theta$ . We first Taylor expand  $\hat{z}_{t+\tau} - z_t$  up to order  $\tau$  terms. To do this, we observe that by our assumptions on  $f, g, h_\theta, u_\theta$ , the functions  $F, G$  are both in  $C^{1,1}$ . Hence,

$$\begin{aligned} F(\bar{z}_{t+\tau}, t + \tau) &= F(z_t, t) + D_Z F(z_t, t)[\bar{z}_{t+\tau} - z_t] + \partial_t F(z_t, t) \tau + O(\|\bar{z}_{t+\tau} - z_t\|^2) + O(\tau^2) \\ &= F(z_t, t) + D_Z F(z_t, t)[G(z_t, t)w] \sqrt{\tau} + O^*(\tau). \end{aligned}$$

Here, both the  $O(\cdot)$  and  $O^*(\cdot)$  notation are the same as in the proof of Lemma 4.1. By a similar argument,

$$G(\bar{z}_{t+\tau}, t + \tau) = G(z_t, t) + D_Z G(z_t, t)[G(z_t, t)w] \sqrt{\tau} + O^*(\tau).$$

Hence,

$$\hat{z}_{t+\tau} - z_t = \left[ F(z_t, t) + \frac{1}{2} D_Z G(z_t, t)[G(z_t, t)w]w \right] \tau + G(z_t, t)w \sqrt{\tau} + O^*(\tau^{3/2}). \quad (4.19)$$

A straightforward computation yields:

$$D_Z G((x, y), t)[(\Delta_x, \Delta_y)] = \begin{bmatrix} Dg(x, t)[\Delta_x] \\ \nabla u(x, t)^\top Dg(x, t)[\Delta_x] + \Delta_x^\top \nabla^2 u(x, t)g(x, t) \end{bmatrix},$$

and therefore:

$$\frac{1}{2} D_Z G(z_t, t) [G(z_t, t) w] w = \frac{1}{2} \left[ \nabla u(x, t)^\top Dg(x, t) [g(x, t) w] w + w^\top g(x, t)^\top \nabla^2 u(x, t) g(x, t) w \right].$$

Substituting the above into expression (4.19) for  $\hat{z}_{t+\tau} - z_t$ ,

$$\begin{aligned} \hat{z}_{t+\tau} - z_t &= \left[ h(x, t) - \frac{1}{2} \text{tr}(H(x, t) \nabla^2 u(x, t)) \right] \tau \\ &\quad + \frac{1}{2} \left[ \nabla u(x, t)^\top Dg(x, t) [g(x, t) w] w + w^\top g(x, t)^\top \nabla^2 u(x, t) g(x, t) w \right] \tau \\ &\quad + \sqrt{\tau} \left[ \frac{g(x, t) w}{\nabla u(x, t)^\top g(x, t) w} \right] + O^*(\tau^{3/2}). \end{aligned} \quad (4.20)$$

Setting  $\bar{\Delta} := (\hat{x}_{t+\tau} - x, \tau) \in \mathbb{R}^{d+1}$  we have:

$$\begin{aligned} u(\hat{x}_{t+\tau}, t + \tau) - u(x, t) &= Du(x, t) \bar{\Delta} + \frac{1}{2} \bar{\Delta}^\top D^2 u(x, t) \bar{\Delta} + O(\|\bar{\Delta}\|^3), \\ Du(x, t) \bar{\Delta} &= \langle \nabla u(x, t), \hat{x}_{t+\tau} - x \rangle + \partial_t u(x, t) \tau, \\ \frac{1}{2} \bar{\Delta}^\top D^2 u(x, t) \bar{\Delta} &= \frac{1}{2} \left( (\hat{x}_{t+\tau} - x)^\top \nabla^2 u(x, t) (\hat{x}_{t+\tau} - x) + 2\tau \langle \partial_t \nabla u(x, t), \hat{x}_{t+\tau} - x \rangle + \tau^2 \partial_t^2 u(x, t) \right), \end{aligned}$$

from which we conclude,

$$\begin{aligned} u(\hat{x}_{t+\tau}, t + \tau) - u(x, t) &= \langle \nabla u(x, t), \hat{x}_{t+\tau} - x \rangle + \partial_t u(x, t) \tau + \frac{1}{2} (\hat{x}_{t+\tau} - x)^\top \nabla^2 u(x, t) (\hat{x}_{t+\tau} - x) + O(\tau^{3/2}) \\ &= \left[ \langle \nabla u(x, t), f(x, t) + \frac{1}{2} Dg(x, t) [g(x, t) w] w \rangle + \partial_t u(x, t) + \frac{1}{2} w^\top g(x, t)^\top \nabla^2 u(x, t) g(x, t) w \right] \tau \\ &\quad + \sqrt{\tau} \langle \nabla u(x, t), g(x, t) w \rangle + O^*(\tau^{3/2}). \end{aligned}$$

On the other hand, from (4.20),

$$\begin{aligned} \hat{y}_{t+\tau} - y_t &= \left[ h(x, t) - \frac{1}{2} \text{tr}(H(x, t) \nabla^2 u(x, t)) \right] \tau \\ &\quad + \frac{1}{2} \left[ \nabla u(x, t)^\top Dg(x, t) [g(x, t) w] w + w^\top g(x, t)^\top \nabla^2 u(x, t) g(x, t) w \right] \tau \\ &\quad + \sqrt{\tau} \nabla u(x, t)^\top g(x, t) w + O^*(\tau^{3/2}). \end{aligned}$$

Hence,

$$\begin{aligned} u(\hat{x}_{t+\tau}, t + \tau) - \hat{y}_{t+\tau} &= (u(\hat{x}_{t+\tau}, t + \tau) - u(x, t)) - (\hat{y}_{t+\tau} - y_t) \\ &= \left[ \langle \nabla u(x, t), f(x, t) \rangle + \partial_t u(x, t) + \frac{1}{2} \text{tr}(H(x, t) \nabla^2 u(x, t)) - h(x, t) \right] \tau + O^*(\tau^{3/2}) \\ &= R[u](x, t) \tau + O^*(\tau^{3/2}). \end{aligned}$$

To conclude,

$$\mathbb{E}_w (u(\hat{x}_{t+\tau}, t + \tau) - \hat{y}_{t+\tau})^2 = \mathbb{E}_w (R[u](x, t) \tau + O^*(\tau^{3/2}))^2 = (R[u](x, t))^2 \tau^2 + O(\tau^{5/2}).$$

□

With Lemma 4.3 in hand, let us further assume that sufficient regularity on the forward SDE (4.6) is in place to ensure the order 1/2 strong convergence of the stochastic Heun method [see e.g. 7, 35], i.e.,<sup>2</sup>

$$\left( \mathbb{E} \left[ \max_{k \in \{0, \dots, N-1\}} \|\hat{X}_k^\bullet - X_{t_k}^\bullet\|^2 \right] \right)^{1/2} \leq C\tau^{1/2}, \quad (4.21)$$

where again  $C$  is independent of  $\tau$  but may depend on  $T$  and the properties of the forward SDE (4.6). We can replicate the arguments in (4.5) and conclude:

$$L_{\text{Heun},\tau}(\theta) = \frac{1}{T} \int_0^T \mathbb{E}(R[u_\theta](X_t^\bullet, t))^2 dt + O(\tau^{1/2}), \quad (4.22)$$

where the  $X_t^\bullet$  in (4.22) is the Stratonovich solution (4.6). Thus unlike the EM case in (4.5), any additional bias terms only enter through a  $O(\tau^{1/2})$  term which is of higher order than the leading PDE residue term. In Figure 1b, we show the plot of  $L_{\text{Heun},\tau}(\theta)$  on the same HJB PDE problem as in Figure 1a, and show that the bias in  $L_{\text{EM},\tau}(\theta)$  is no longer present.

## 5 Trade-offs of Long Horizons Losses for BSDEs

In Section 4, we conduct a thorough analysis of the one-step consistency losses  $L_{\text{BSDE},\tau}(\theta)$  and  $L_{\text{S-BSDE},\tau}(\theta)$  and their corresponding EM and Heun discrete counterparts,  $L_{\text{EM},\tau}(\theta)$  and  $L_{\text{Heun},\tau}(\theta)$ , respectively. We now turn to studying the generalized losses  $L_{\text{BSDE}}(\theta)$  and  $L_{\text{S-BSDE}}(\theta)$ . In this section, for the generalized BSDE and S-BSDE losses we will analyze time distributions  $(t_s, t_f) \sim \rho$  satisfying  $t_s = 0$  and  $t_f = T$ ; the intermediate regime is studied experimentally in Section 6.

**BSDE loss and Euler-Maruyama discretization.** We start with the BSDE loss (3.7). By application of Itô's Lemma, we have for  $u_\theta(x, t)$ ,

$$u_\theta(X_T, T) - u_\theta(X_0, 0) - \int_0^T h_\theta(X_t, t) dt - \int_0^T \nabla u_\theta(X_t, t)^\top g(X_t, t) dB_t = \int_0^T R[u_\theta](X_t, t) dt,$$

which immediately yields the following identity:

$$L_{\text{BSDE}}(\theta) = \mathbb{E}_{x_0 \sim \mu_0, B_t} \left( \frac{1}{T} \int_0^T R[u_\theta](X_t, t) dt \right)^2. \quad (5.1)$$

Thus, the BSDE loss is equal to averaging the square of the accumulation of the residual error  $R[u_\theta]$  along the forward SDE trajectories. Hence by Jensen's inequality, the BSDE loss is dominated by the following forwards SDE PINNs loss:

$$L_{\text{BSDE}}(\theta) \leq \mathbb{E}_{x_0 \sim \mu_0, B_t} \frac{1}{T} \int_0^T (R[u_\theta](X_t, t))^2 dt =: L_{\text{FS-PINNs}}(\theta). \quad (5.2)$$

Next, assuming enough regularity on  $R[u_\theta]$ , we have

$$\mathbb{E} \left( \int_{t_k}^{t_{k+1}} R[u_\theta](X_t, t) dt \right)^2 = \tau^2 \mathbb{E}[R[u_\theta]^2(X_{t_k}, t_k)] + O(\tau^3). \quad (5.3)$$

---

<sup>2</sup>In the general multi-dimensional setting, the order of strong convergence of the stochastic Heun method is only 1/2; order 1 is only achieved in either the scalar case, or when the drift term of the SDE satisfies a commutativity condition (which happens when the drift is e.g., constant). See [7] for a more detailed discussion.

Therefore,

$$\begin{aligned}
L_{\text{BSDE},\tau}(\theta) &= \mathbb{E}_{x_0 \sim \mu_0, B_t} \frac{1}{N\tau^2} \sum_{k=0}^{N-1} \left( \int_{t_k}^{t_{k+1}} R[u_\theta](X_t, t) dt \right)^2 \\
&= \mathbb{E}_{x_0 \sim \mu_0, B_t} \frac{1}{N\tau^2} \sum_{k=0}^{N-1} (\tau^2 R[u_\theta]^2(X_{t_k}, t_k) + O(\tau^3)) \quad [\text{using (5.3)}] \\
&= \mathbb{E}_{x_0 \sim \mu_0, B_t} \frac{1}{N} \sum_{k=0}^{N-1} R[u_\theta]^2(X_{t_k}, t_k) + O(\tau) \\
&= \mathbb{E}_{x_0 \sim \mu_0, B_t} \frac{1}{T} \int_0^T (R[u_\theta](X_t, t))^2 dt + O(\tau) \\
&= L_{\text{FS-PINNs}}(\theta) + O(\tau),
\end{aligned}$$

where the penultimate equality holds from the standard approximation properties of a left Riemann sum to the Riemann integral. Thus, we have the following relationship between the two BSDE losses:

$$L_{\text{BSDE}}(\theta) \leq L_{\text{BSDE},\tau}(\theta) + O(\tau). \quad (5.4)$$

Thus, at the SDE level, the benefits of using the more general BSDE loss  $L_{\text{BSDE}}(\theta)$  over the one-step BSDE loss  $L_{\text{BSDE},\tau}(\theta)$  are not obvious, given that (a) the general BSDE loss is dominated by the one-step self-consistency loss (up to an order  $\tau$  term) as in (5.4), and (b)  $L_{\text{BSDE},\tau}(\theta)$  does indeed vanish for an optimal solution  $\theta_*$ . Note that while the relationship in (5.2) is pointed out in [5, Section 5.2.3], the implications of this inequality in (5.4) are not discussed in their work.

While the relationships at the SDE level between the various losses are now clear given the context of our discussion, the situation becomes a bit murkier when factoring in EM discretization. Assuming sufficient regularity for the order 1/2 strong convergence of EM jointly on  $(X_t, Y_t^\theta)$ , i.e.,

$$\left( \mathbb{E} \left[ \max_{k \in \{0, \dots, N-1\}} \max \{ \|\hat{X}_k - X_{t_k}\|^2, |\hat{Y}_k^\theta - Y_{t_k}^\theta|^2 \} \right] \right)^{1/2} \leq C\tau^{1/2},$$

in addition to sufficient regularity of  $u_\theta$  and the moments of  $(X_T, Y_T^\theta)$  and  $(\hat{X}_N, \hat{Y}_N^\theta)$ ,

$$\begin{aligned}
L_{\text{EM}}(\theta) &= \mathbb{E}_{x_0 \sim \mu_0, w_k} \frac{1}{T^2} \left( u_\theta(\hat{X}_N, T) - u_\theta(x_0, 0) - (\hat{Y}_N^\theta - \hat{Y}_0^\theta) \right)^2 \\
&= \mathbb{E}_{x_0 \sim \mu_0, B_t} \frac{1}{T^2} \left( u_\theta(X_T, T) - u_\theta(x_0, 0) - (Y_T^\theta - Y_0^\theta) \right)^2 + O(\tau^{1/2}) \\
&= L_{\text{BSDE}}(\theta) + O(\tau^{1/2}). \quad (5.5)
\end{aligned}$$

Hence the error between the EM discretized loss  $L_{\text{EM}}(\theta)$  and the idealized SDE loss  $L_{\text{BSDE}}(\theta)$  can be made arbitrarily small by decreasing the step size  $\tau$ . On the other hand, (4.5) shows that

$$\begin{aligned}
L_{\text{EM},\tau}(\theta) &= L_{\text{BSDE},\tau}(\theta) + \text{Bias}(\theta) + O(\tau^{1/2}), \\
\text{Bias}(\theta) &:= \frac{1}{2T} \int_0^T \mathbb{E} \text{tr}((H(X_t, t) \cdot \nabla^2 u_\theta(X_t, t))^2) dt,
\end{aligned}$$

with  $\text{Bias}(\theta)$  not vanishing as  $\tau \rightarrow 0$ . Hence, the loss  $L_{\text{EM}}(\theta)$  present an advantage over  $L_{\text{EM},\tau}(\theta)$  for sufficiently small discretization sizes in terms of controllable bias. However, the inequality from (5.4) still holds, meaning that while  $L_{\text{EM}}(\theta)$  does not suffer from the bias issues identified in  $L_{\text{EM},\tau}(\theta)$ , the trade-off is that the loss it approximates well is not necessarily the best loss to use. On the other hand, while  $L_{\text{EM},\tau}(\theta)$  attempts to approximate the stronger loss  $L_{\text{BSDE},\tau}(\theta)$ , it does so in a way that introduces a bias term  $\text{Bias}(\theta)$  which cannot be reduced with small enough  $\tau$ . Thus, neither of the losses provides a completely satisfactory solution in practice. In Section 6.2.2, we illustrate the issues with the  $L_{\text{EM}}(\theta)$  loss empirically.

**Stratonovich BSDE and Heun discretization.** We now consider the case of Stratonovich BSDEs and the Heun discretization. From the Stratonovich chain rule

$$\begin{aligned} u_\theta(X_T^\bullet, T) - u_\theta(X_0^\bullet, 0) &= \int_0^T \left[ R[u_\theta](X_t^\bullet, t) + h_\theta(X_t^\bullet, t) - \frac{1}{2} \text{tr}(H(X_t^\bullet, t) \nabla^2 u_\theta(X_t^\bullet, t)) \right] dt \\ &\quad + \int_0^T \nabla u_\theta(X_t^\bullet, t)^\top g(X_t^\bullet, t) \circ dB_t, \end{aligned}$$

and hence we have the following identity which parallels (5.1):

$$L_{\text{S-BSDE}}(\theta) = \mathbb{E}_{x_0 \sim \mu_0, B_t} \left( \frac{1}{T} \int_0^T R[u_\theta](X_t^\bullet, t) dt \right)^2.$$

Assuming sufficient regularity and using nearly identical arguments as for (5.4), a similar inequality holds for the Stratonovich BSDE loss:

$$L_{\text{S-BSDE}}(\theta) \leq L_{\text{S-BSDE}, \tau}(\theta) + O(\tau).$$

However, when we consider discretizing the Stratonovich integrals with Heun integration, we see a different conclusion than with the EM case. We first start by assuming enough regularity for order 1/2 strong convergence of Heun on the joint SDE  $(X_t^\bullet, Y_t^{\bullet, \theta})$ :

$$\left( \mathbb{E} \left[ \max_{k \in \{0, \dots, N-1\}} \max \{ \|\hat{X}_k^\bullet - X_{t_k}^\bullet\|^2, |\hat{Y}_k^{\bullet, \theta} - Y_{t_k}^{\bullet, \theta}|^2 \} \right] \right)^{1/2} \leq C\tau^{1/2},$$

in addition to sufficient regularity of  $u_\theta$  and the moments of  $(X_T^\bullet, Y_T^{\bullet, \theta})$  and  $(\hat{X}_N^\bullet, \hat{Y}_N^{\bullet, \theta})$ . Then, following the arguments deriving (5.5), we have  $L_{\text{Heun}}(\theta) = L_{\text{S-BSDE}}(\theta) + O(\tau^{1/2})$ . The key difference, however, between the EM and Heun discretization is that for  $L_{\text{S-BSDE}, \tau}(\theta)$ , from (4.22) we have the more favorable identity  $L_{\text{Heun}, \tau}(\theta) = L_{\text{S-BSDE}, \tau}(\theta) + O(\tau^{1/2})$ . Hence unlike the EM setting, both  $L_{\text{Heun}}(\theta)$  and  $L_{\text{Heun}, \tau}(\theta)$  can be made arbitrarily close to their SDE counterparts for sufficiently small  $\tau$ , and hence:

$$L_{\text{Heun}}(\theta) \leq L_{\text{Heun}, \tau}(\theta) + O(\tau^{1/2}).$$

This parallels the inequality (5.4) for the BSDE loss, and suggests questionable benefits of  $L_{\text{Heun}}(\theta)$  over  $L_{\text{Heun}, \tau}(\theta)$ . In Section 6.2.2, we show that this conclusion is indeed reflected in practice.

## 6 Experiments

In this section, we compare the proposed Heun-based BSDE methods against both standard PINNs, a variant of PINNs which uses the forward SDE to sample collocation points, and standard Euler-Maruyama based BSDE solvers, on various high-dimensional PDE problems. Specifically, we compare the following approaches:

- (a) **PINNs:** The standard PINNs loss, i.e.,  $L_{\text{PINNs}}$  from (3.4), is minimized. Since the domain  $\Omega$  is unbounded here, the measure  $\mu$  over space-time  $(x, t)$  is chosen by fitting a normal distribution over the spatial dimensions of the forward SDE trajectories prior to training. For coupled FBSEEs, the analytical solution was utilized in determining this distribution as the forward SDE is dependent on the target solution of the BSDE.
- (b) **FS-PINNs:** The standard PINNs loss (3.4) is again minimized. However, the measure  $\mu$  over space-time is chosen by directly sampling trajectories from the forward SDE, as is written in (5.2).
- (c) **EM-BSDE:** The one-step self-consistency loss discretized with the standard Euler-Maruyama scheme, i.e.,  $L_{\text{EM}, \tau}$  from (3.12).

(d) **EM-BSDE (NR):** A variant of EM-BSDE where we use the BSDE to propagate  $Y_t$  instead of setting it directly to  $u_\theta(X_t, t)$ . We refer to this variant as the *no-reset* (NR) variant. Specifically, the backwards SDEs in (3.10) is integrated as:

$$\hat{Y}_{k+1}^\theta = \hat{Y}_k^\theta + h(\hat{X}_k, t_k, \hat{Y}_k^\theta, \nabla u_\theta(\hat{X}_k, t_k))\tau + \sqrt{\tau} \nabla u_\theta(\hat{X}_k, t_k)^\top g(\hat{X}_k, t_k) w_k, \quad \hat{Y}_0^\theta = u_\theta(x_0, 0). \quad (6.1)$$

The loss  $L_{\text{EM}, \tau}$  remains the same as (3.12), except replacing (3.10) with (6.1).

(e) **Heun-BSDE:** The one-step self-consistency loss discretized with stochastic Heun integration, i.e.,  $L_{\text{Heun}, \tau}$  from (4.13).

We use each algorithm to train an 8-layer neural network with 64 neurons per layer and swish activation to model the solution  $u(x, t)$  of a PDE. The boundary condition (3.2) is enforced by adding a boundary condition penalty  $\mathbb{E}_{x \sim \mu'}[(u_\theta(x, T) - \phi(x)^2) + \mathbb{E}[\|\nabla u_\theta(x, T) - \nabla \phi(x)\|^2]]$  involving both the zero-th and first-order values of  $\phi$  [4], where the distribution  $\mu'$  is taken over each method's approximation of the distribution of  $X_T$ . Additionally, following state-of-the-art PINN architectures practices [2], Fourier embeddings [36] with a 256 embedding dimension and skip connections on odd layers are used. In most of our experiments, the time domain  $[0, T]$  is discretized into 50 equally space intervals with a batch size of 64, translating to 64 realizations of the underlying Brownian motions; we also include a study where the  $[0, T]$  is discretized into 200 equally spaced intervals to study the effects of finer discretization. Furthermore, even though the EM-BSDE, EM-BSDE (NR), and Heun-BSDE methods described here all employ single-step self-consistency losses, we also conduct an experiment where longer horizon self-consistency losses are utilized; we defer the implementation details of these methods in the longer horizon setting for now. We use the Adam optimizer with a multi-step learning rate schedule [4] of  $10^{-3}$ ,  $10^{-4}$ , and  $10^{-5}$  at 50k, 75k, and 100k iterations, respectively. To evaluate the model performance, the analytical solution is computed and compared with the model output along 5 forward SDE trajectories, using the *relative  $L_2$  error* (RL2) metric:

$$\text{RL2} := \sqrt{\frac{\sum_{i=0}^{N-1} (u_{\text{ref}}(X_{t_i}, t_i) - u_{\text{pred}}(X_{t_i}, t_i))^2}{\sum_{i=0}^{N-1} u_{\text{ref}}^2(X_{t_i}, t_i)}}.$$

All models are trained on a single NVIDIA A100 GPU, using the `jax` library [37]. Code to reproduce our experiments is available at: <https://github.com/sungje-park/heunbsde>

## 6.1 PDE Test Cases

**Hamilton-Jacobi-Bellman (HJB) Equation.** First, we consider the following Hamilton-Jacobi-Bellman (HJB) equation studied in [4]:

$$\partial_t u(x, t) = -\text{Tr}[\nabla^2 u(x, t)] + \|\nabla u(x, t)\|^2, \quad x \in \mathbb{R}^d, \quad t \in [0, T].$$

For the terminal condition  $u(x, T) = g(x) = \ln(.5(1 + \|x\|^2))$ , the analytical solution is given as

$$u(x, t) = -\ln \left( \mathbb{E} \left[ \exp \left( -g(x + \sqrt{2}B_{T-t}) \right) \right] \right). \quad (6.2)$$

The HBJ PDE is related to the forward-backward stochastic differential equation of the form:

$$\begin{aligned} dX_t &= \sigma dB_t, \quad t \in [0, T], \\ dY_t &= \|Z_t\|^2 dt + \sigma Z_t^\top dB_t, \quad t \in [0, T], \end{aligned}$$

where  $T = 1$ ,  $\sigma = \sqrt{2}$ ,  $X_0 = 0$ , and  $Y_T = g(X_T)$ . In our experiments, in order to compute the analytical solution (6.2), we approximate it using  $10^5$  Monte-Carlo samples.

**Black-Scholes-Barenblatt (BSB) Equation.** Next, we consider the 100D Black-Scholes-Barenblatt (BSB) equation from [4] of the form

$$\partial_t u(x, t) = -\frac{1}{2} \text{Tr}[\sigma^2 \text{diag}(x^2) \nabla^2 u(x, t)] + r(u(x, t) - \nabla u(x, t)^\top x), \quad x \in \mathbb{R}^d, \quad t \in [0, T],$$

where  $x^2$  is understood to be coordinate-wise, and  $\text{diag}(v)$  is a diagonal matrix with  $\text{diag}(v)_i = v_i$ . Given the terminal condition  $u(x, T) = g(x) = \|x\|^2$ , the explicit solution to this PDE is

$$u(x, t) = \exp((r + \sigma^2)(T - t)) g(x).$$

The BSB PDE is related to the following FBSDE

$$\begin{aligned} dX_t &= \sigma \text{diag}(X_t) dB_t, \quad t \in [0, T], \\ dY_t &= r(Y_t - Z_t^\top X_t) dt + \sigma Z_t^\top \text{diag}(X_t) dB_t, \quad t \in [0, T], \end{aligned}$$

where  $T = 1$ ,  $\sigma = .4$ ,  $r = .05$ ,  $X_0 = (1, .5, 1, .5, \dots, 1, .5)$ , and  $Y_T = g(X_T)$ .

**Fully-Coupled FBSDE.** Finally, we consider a FBSDE with *coupled* forward and backwarwds dynamics adapted from Bender & Zhang (BZ) [38]:

$$\begin{aligned} dX_t &= \sigma Y_t dB_t, \quad t \in [0, T], \\ dY_t &= -r Y_t + \frac{1}{2} e^{-3r(T-t)} \sigma^2 \left( D \sum_{j=0}^d \sin(X_{j,t}) \right)^3 dt + Z_t^\top dB_t, \quad t \in [0, T], \end{aligned}$$

where  $X_{j,t}$  denotes the  $j$ -th coordinate of  $X_t \in \mathbb{R}^d$ . Due to the dependence of the forward process  $(X_t)$  on  $(Y_t)$ , this set of coupled FBSDE does not fit into the mathematical formulation set forth in (3.5) and (3.6). Nevertheless, we can still apply the BSDE methods described at the beginning of Section 6 by initializing  $Y_0 = u_\theta(x, 0)$  and jointly integrating  $(X_t, Y_t)$ . We set  $T = 1$ ,  $r = .1$ ,  $\sigma = .3$ ,  $D = .1$ ,  $X_0 = (\pi/2, \pi/2, \dots, \pi/2)$ , and  $Y_T(X_T) = g(X_T) = D \sum_{j=1}^d \sin(X_{j,T})$ . The above FBSDE is induced from the following PDE

$$\partial_t u(x, t) = -\frac{1}{2} \sigma^2 u(x, t)^2 \nabla^2 u(x, t) + r u(x, t) - \frac{1}{2} e^{-3r(T-t)} \sigma^2 \left( D \sum_{j=0}^d \sin(x_j) \right)^2$$

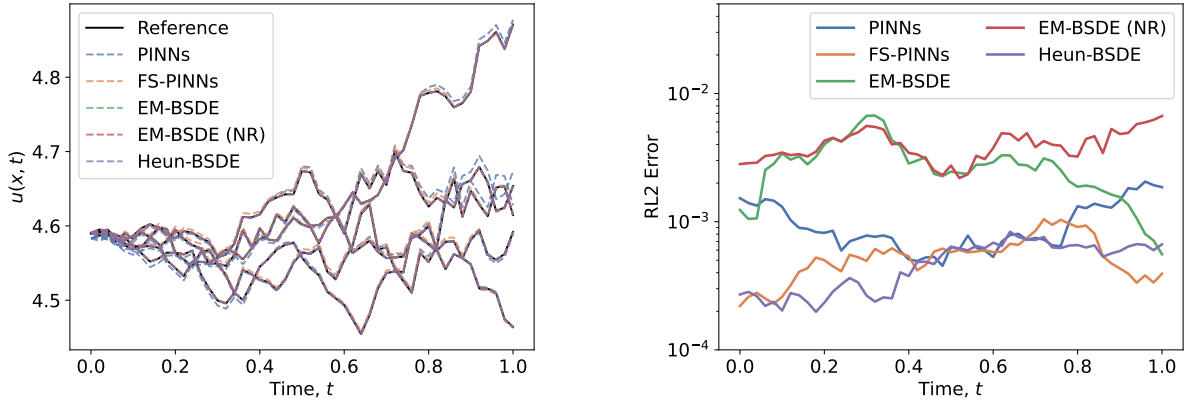
with the analytical solution  $u(x, t) = e^{-r(T-t)} D \sum_{j=0}^d \sin(x_j)$ .

## 6.2 Results

We report three sets of results on one-step self-consistency losses (Section 6.2.1), multi-step self-consistency losses (Section 6.2.2), and the effects of floating point precision (Section 6.2.3).

### 6.2.1 One-Step Self-Consistency Losses

For our first set of results, we solve each PDE from Section 6.1 instantiated with a state space of 100 dimensions; each case is ran with three different initialization seeds. The results are reported in Table 1, which shows that for nearly all the cases, the Heun-BSDE method outperforms EM-BSDE methods (lower RL2 error) as predicted by our analysis in Section 4. Furthermore, Figure 2 illustrates the performance of all methods across the time axis on the 100D HJB case, which also highlights the low RL2 error of the Heun-BSDE method. The one exception to the trend is the 100D BZ case, where all methods failed to converge on a satisfactory solution. We hypothesize due to the complexity of the problem, the optimization landscape of each method is too complex to recovery high-quality solutions. To evaluate this hypothesis, we reduce the dimensionality of



(a) Plot of the learned solution of different models on the 100D HJB problem.

(b) Plot of the RL2 errors at each discretization step for the 100D HJB case.

**Figure 2:** A plot of the 100D HJB reference and learned solutions for each model and the associated RL2 errors.

Cases	PINNs	FS-PINNs	EM-BSDE (NR)	EM-BSDE	Heun-BSDE
100D HJB	$0.1260 \pm 0.0107$	$0.0737 \pm .0110$	$0.5214 \pm .0452$	$0.3626 \pm .0113$	<b><math>0.0493 \pm .0109</math></b>
100D BSB	$1.5066 \pm 0.2349$	<b><math>0.0497 \pm .0031</math></b>	$0.1855 \pm 0.0078$	$0.3735 \pm 0.0470$	$0.0535 \pm 0.0113$
100D BZ	-	-	-	<b><math>3.1259 \pm 0.1807</math></b>	$3.5619 \pm 0.2716$
10D BZ	$3.8566 \pm 0.0310$	$0.0351 \pm 0.0041$	$0.1309 \pm 0.0311$	$0.1903 \pm 0.0066$	<b><math>0.0228 \pm 0.0016</math></b>

**Table 1:** Summary of RL2 errors averaged over three different initialization random seeds. Settings that failed to converge to a satisfactory solution are denoted with -.

the BZ problem to 10D and re-run all methods, which restores the performance of Heun-BSDE. Another key observation from Table 1 is that FS-PINNs and Heun-BSDE perform similarly across all cases, showing that parity between the BSDE and PINNs method is restored through Heun integration. Finally, we note that the performance of PINNs is quite poor in comparison to FS-PINNs, which illustrates the importance of the space-time sampling distribution  $\mu$  for PINNs based methods.

To show that the gap between EM-BSDE and Heun-BSDE cannot be closed with finer discretization meshes, we re-run the 10D BSB example at varying discretization sizes. The results are reported in Figure 3, which show that the EM-BSDE methods only experience minimal improvement with smaller discretization size compared with the Heun-BSDE method.

Cases	PINNs	FS-PINNs	EM-BSDE (NR)	EM-BSDE	Heun-BSDE
100D HJB	$1243 \pm 12$	$2456 \pm 109$	$2159 \pm 13$	$2188 \pm 13$	$49005 \pm 2034$
100D BSB	$1248 \pm 15$	$2666 \pm 13$	$2316 \pm 4$	$2323 \pm 6$	$52920 \pm 267$
100D BZ	$1257 \pm 19$	$3499 \pm 16$	$2425 \pm 19$	$2442 \pm 19$	$49808 \pm 123$
10D BZ	$379 \pm 11$	$1383 \pm 8$	$2159 \pm 6$	$2177 \pm 5$	$9094 \pm 13$
vs PINNs	<b>1x</b>	<b>2.64x</b>	<b>2.81x</b>	<b>2.83x</b>	<b>36.37x</b>

**Table 2:** Average training time on each tested configuration (in seconds) using NVIDIA A100 GPUs. The last column represents the average overhead vs PINNs.

**Computational considerations.** Although Heun-BSDE outperforms EM-BSDE, it comes at the cost of computational requirements due to the mechanics of Heun integration. In Table 2, we report the average

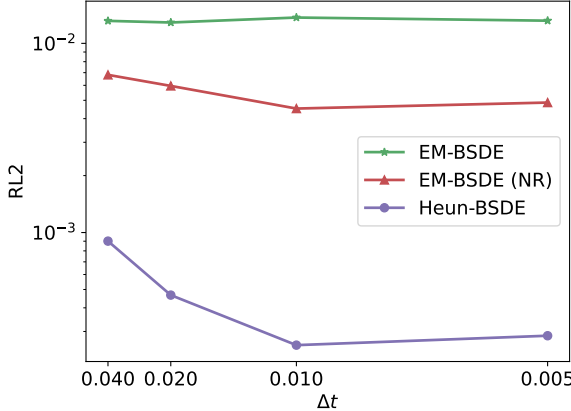


**Figure 3:** A plot of RL2 performance of the 10D BSB case at various discretization step-sizes.

training time for each method on a single NVIDIA A100 GPU. Table 2 shows that on average, Heun-BSDE is over 20 times slower than the EM-BSDE method. This is because the Heun discretization requires three times as many samples from the NN per discretization step and explicit computation of the Hessian,  $\nabla^2 u(x, t)$  which results in both significant memory requirements and also higher sensitivity to floating point precision (which we show in Section 6.2.3). We leave investigating more sophisticated implementations, including e.g., the use of the Hutchinson trace estimator to improve the speed of the Hessian computations as is done for PINNs [39], and the use of other Heun integrators such as reversible Heun [35], to future work.

### 6.2.2 Multi-Step Self-Consistency Losses

We next consider multi-step self-consistency BSDE losses in order to evaluate the mathematical analysis conducted in Section 5. Specifically, we vary the horizon length in the following way. Let  $k \in \{1, \dots, N-1\}$  denote the *skip-length*. We then define the distribution  $(t_s, t_f) \sim \rho_k$  (cf. (3.7)) over start and end times as

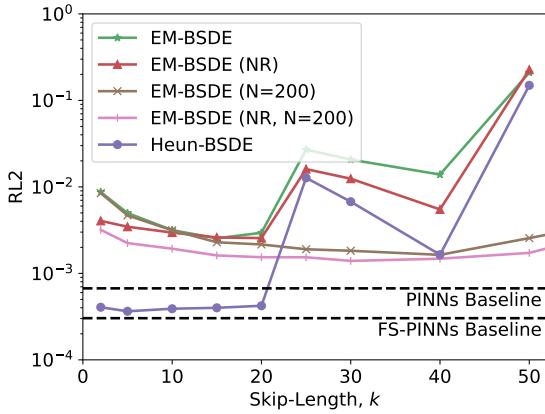
$$t_s \sim \text{Unif}(\{t_{ik} \mid i \in \mathbb{N}, ik \leq N-1\}), \quad t_f = \min\{t_s + k, N\}.$$

We then use  $L_{\text{EM}}$  (cf. (4.12)) with the choice of  $\rho = \rho_k$ . The next thing we need to determine is where both EM-BSDE and EM-BSDE (NR) will ‘reset’ the value of  $Y_t$  to  $u_\theta(X_t, t)$ . Note that there are many degrees of freedom here in the multi-step formulation, so we simply pick one choice as a representative choice. For EM-BSDE, we set  $Y_{t_s} = u_\theta(X_{t_s}, t_s)$ , and use (6.1) to integrate between  $t_s$  and  $t_f$ . On the other hand, for EM-BSDE (NR), we directly use the value of  $Y_{t_s}$ . We also compare EM-BSDE and EM-BSDE (NR) with  $N$ , the number of discretization steps for the interval  $[0, T]$ , varying between  $N \in \{50, 200\}$  as well. We conduct this experiment on the 10D BSB setting, with the results reported in Figure 4.

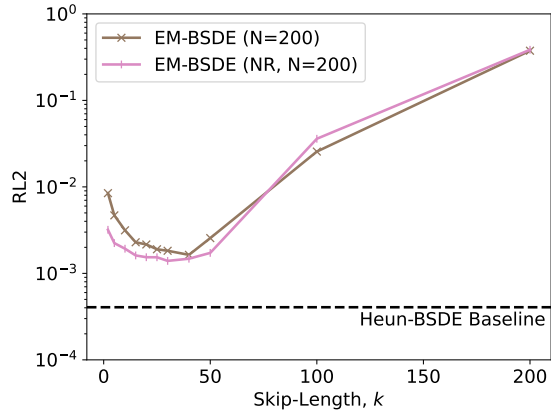
Figure 4 shows that while the Heun-BSDE performance decreases as the skip-length increases, the performance of both EM-BSDE methods initially improves with skip-length before degrading, demonstrating a clear trade-off between minimizing the bias term and decreasing quality of the self-regularization loss identified in Section 5. Although the EM-BSDE method improves by optimizing the skip-length  $k$ , the best Heun-BSDE model still outperformed the best EM-BSDE model by a significant margin.

### 6.2.3 Sensitivity to Floating Point Precision

In BSDE-based losses, floating point errors can accumulate through out integration of the SDEs, leading to poor performance on the trained model. As seen in Table 3, the floating point error is especially apparent in the Heun loss where the performance of the model is improved by a factor of 10 between `float32` and `float64`. In addition, performance improvements were observed for the PINNs and FS-PINNs models as well.



(a) Plot of RL2 performance as a function of the skip-length  $k$ , with the number of discretization steps also varying in  $N \in \{50, 200\}$ .



(b) Plot of RL2 performance as a function of the skip-length  $k$  for EM-BSDE and EM-BSDE (NR), with number of discretization steps set to  $N = 200$ .

**Figure 4:** A plot of RL2 performance at various skip lengths. The RL2 performance of each model on the 10D BSB case was averaged from three runs with varying initializations. Trajectory length represents the number of discretization steps in  $[0, T]$  and is inversely proportional to the step size  $\tau$ .

It is also noted that the EM-BSDE models performed slightly worse at a `float64`, which may be attributed to the bias term present in its loss. We leave more numerically stable implementations of the Heun solver in `float32`, such as PDE non-dimensionalization [2] and the use of the reversible Heun solver from [35], to future work.

Method	float32	float64
PINNs	$2.9648 \pm 0.8652$	$1.5066 \pm 0.2349$
FS-PINNs	$0.0602 \pm .0150$	$0.0497 \pm .0031$
EM-BSDE	$0.2451 \pm 0.0160$	$0.3735 \pm .0470$
EM-BSDE (NR)	$0.1648 \pm 0.0143$	$0.1855 \pm .0078$
Heun-BSDE	$0.4587 \pm .0261$	$0.0535 \pm .0113$

**Table 3:** `float32` vs `float64` Performance in 100D BSB

## 7 Conclusion and Future Work

We conducted a systematic study of stochastic discretization strategies for BSDE-based loss formulations used to solve high-dimensional PDEs through deep learning. By comparing the commonly used Euler-Maruyama scheme with stochastic Heun integration, we demonstrated that the choice of discretization can significantly impact the accuracy of BSDE-based methods. Our theoretical analysis showed that EM discretization introduces a non-trivial bias to the single-step self-consistency BSDE loss which does not vanish as the step-size decrease. On the other hand, we show that this bias issue is not present when utilizing Heun discretization. Finally, the empirical results confirmed that the Heun scheme consistently outperforms EM in solution accuracy and performs competitively with PINNs.

These findings underscore the importance of stochastic integrator choice in deep-learning based BSDE solvers and suggest that higher-order schemes—though significantly more computationally intensive—can offer substantial gains in performance. In future works, we aim to reduce Heun-BSDE’s computational costs through methods such as Hutchinson trace estimation [39], reversible Heun [35], and adaptive time-stepping.

Furthermore, while this current work focuses on understanding and restoring performance parity between BSDE and PINNs methods, future work will utilize the advantages of BSDE methods to solve problems such as high-dimensional stochastic control problems in model-free settings.

### Acknowledgments

The authors acknowledge the support of the USC Viterbi Summer Undergraduate Research Experience (SURE) program, which supported S. Park during the beginning stages of this research.

## References

- [1] Maziar Raissi, Paris Perdikaris, and George Em Karniadakis. Physics-informed neural networks: A deep learning framework for solving forward and inverse problems involving nonlinear partial differential equations. *Journal of Computational Physics*, 378:686–707, 2019.
- [2] Sifan Wang, Shyam Sankaran, Hanwen Wang, and Paris Perdikaris. An expert’s guide to training physics-informed neural networks. *arXiv preprint arXiv:2308.08468*, 2023.
- [3] Weinan E, Jiequn Han, and Arnulf Jentzen. Deep learning-based numerical methods for high-dimensional parabolic partial differential equations and backward stochastic differential equations. *Communications in Mathematics and Statistics*, 5(4):349–380, 2017.
- [4] Maziar Raissi. Forward–backward stochastic neural networks: deep learning of high-dimensional partial differential equations. In *Peter Carr Gedenkschrift: Research Advances in Mathematical Finance*, pages 637–655. World Scientific, 2024.
- [5] Nikolas Nüsken and Lorenz Richter. Interpolating between bsdes and pinns: Deep learning for elliptic and parabolic boundary value problems. *Journal of Machine Learning*, 2(1):31–64, 2023.
- [6] Yutian Wang and Yuan-Hua Ni. Deep bsde-ml learning and its application to model-free optimal control, 2022.
- [7] W. Rümelin. Numerical treatment of stochastic differential equations. *SIAM Journal on Numerical Analysis*, 19(3):604–613, 1982.
- [8] Maziar Raissi, Paris Perdikaris, and George Em Karniadakis. Physics informed deep learning (part i): Data-driven solutions of nonlinear partial differential equations. *arXiv preprint arXiv:1711.10561*, 2017.
- [9] Maziar Raissi, Paris Perdikaris, and George Em Karniadakis. Physics informed deep learning (part ii): Data-driven discovery of nonlinear partial differential equations. *arXiv preprint arXiv:1711.10566*, 2017.
- [10] Weinan E and Bing Yu. The deep ritz method: a deep learning-based numerical algorithm for solving variational problems. *Communications in Mathematics and Statistics*, 6(1):1–12, 2018.
- [11] Justin Sirignano and Konstantinos Spiliopoulos. Dgm: A deep learning algorithm for solving partial differential equations. *Journal of Computational Physics*, 375:1339–1364, 2018.
- [12] Nikola Kovachki, Zongyi Li, Burigede Liu, Kamyar Azizzadenesheli, Kaushik Bhattacharya, Andrew Stuart, and Anima Anandkumar. Neural operator: Learning maps between function spaces with applications to pdes. *Journal of Machine Learning Research*, 24(89):1–97, 2023.
- [13] Aditi Krishnapriyan, Amir Gholami, Shandian Zhe, Robert Kirby, and Michael W Mahoney. Characterizing possible failure modes in physics-informed neural networks. In *Advances in Neural Information Processing Systems*, volume 34, pages 26548–26560. Curran Associates, Inc., 2021.

[14] Pratik Rathore, Weimu Lei, Zachary Frangella, Lu Lu, and Madeleine Udell. Challenges in training pinns: a loss landscape perspective. In *Proceedings of the 41st International Conference on Machine Learning*, ICML'24. JMLR.org, 2024.

[15] Sifan Wang, Xinling Yu, and Paris Perdikaris. When and why pinns fail to train: A neural tangent kernel perspective. *Journal of Computational Physics*, 449:110768, 2022.

[16] Chenxi Wu, Min Zhu, Qinyang Tan, Yadhu Kartha, and Lu Lu. A comprehensive study of non-adaptive and residual-based adaptive sampling for physics-informed neural networks. *Computer Methods in Applied Mechanics and Engineering*, 403:115671, 2023.

[17] Haixu Wu, Huakun Luo, Yuezhou Ma, Jianmin Wang, and Mingsheng Long. Ropinn: Region optimized physics-informed neural networks. *arXiv preprint arXiv:2405.14369*, 2024.

[18] Chuwei Wang, Shanda Li, Di He, and Liwei Wang. Is  $L^2$  physics informed loss always suitable for training physics informed neural network? In *Advances in Neural Information Processing Systems*, volume 35, pages 8278–8290. Curran Associates, Inc., 2022.

[19] Zhiwei Gao, Liang Yan, and Tao Zhou. Failure-informed adaptive sampling for pinns. *SIAM Journal on Scientific Computing*, 45(4):A1971–A1994, 2023.

[20] Rambod Mojgani, Maciej Balajewicz, and Pedram Hassanzadeh. Lagrangian pinns: A causality-conforming solution to failure modes of physics-informed neural networks. *arXiv preprint arXiv:2205.02902*, 2022.

[21] Jiequn Han, Arnulf Jentzen, and Weinan E. Solving high-dimensional partial differential equations using deep learning. *Proceedings of the National Academy of Sciences*, 115(34):8505–8510, 2018.

[22] Côme Huré, Huyêñ Pham, and Xavier Warin. Deep backward schemes for high-dimensional nonlinear pdes. *Mathematics of Computation*, 89(324):1547–1579, 2020.

[23] Christian Beck, Weinan E, and Arnulf Jentzen. Machine learning approximation algorithms for high-dimensional fully nonlinear partial differential equations and second-order backward stochastic differential equations. *Journal of Nonlinear Science*, 29:1563–1619, 2019.

[24] Akihiko Takahashi, Yoshifumi Tsuchida, and Toshihiro Yamada. A new efficient approximation scheme for solving high-dimensional semilinear pdes: Control variate method for deep bsde solver. *Journal of Computational Physics*, 454:110956, 2022.

[25] Kristoffer Andersson, Adam Andersson, and C. W. Oosterlee. Convergence of a robust deep fbsde method for stochastic control. *SIAM Journal on Scientific Computing*, 45(1):A226–A255, 2023.

[26] Zebang Shen, Zhenfu Wang, Satyen Kale, Alejandro Ribeiro, Amin Karbasi, and Hamed Hassani. Self-consistency of the fokker planck equation. In *Proceedings of Thirty Fifth Conference on Learning Theory*, volume 178 of *Proceedings of Machine Learning Research*, pages 817–841. PMLR, 02–05 Jul 2022.

[27] Nicholas M Boffi and Eric Vanden-Eijnden. Probability flow solution of the fokker–planck equation. *Machine Learning: Science and Technology*, 4(3):035012, 2023.

[28] Lingxiao Li, Samuel Hurault, and Justin M Solomon. Self-consistent velocity matching of probability flows. In *Advances in Neural Information Processing Systems*, volume 36, pages 57038–57057. Curran Associates, Inc., 2023.

[29] I.E. Lagaris, A. Likas, and D.I. Fotiadis. Artificial neural networks for solving ordinary and partial differential equations. *IEEE Transactions on Neural Networks*, 9(5):987–1000, 1998.

- [30] Aditya Singh, Zeyuan Feng, and Somil Bansal. Exact imposition of safety boundary conditions in neural reachable tubes. *arXiv preprint arXiv:2404.00814*, 2024.
- [31] Quentin Chan-Wai-Nam, Joseph Mikael, and Xavier Warin. Machine learning for semi linear pdes. *Journal of Scientific Computing*, 79(3):1667–1712, 2019.
- [32] Lorenc Kapllani and Long Teng. Deep learning algorithms for solving high-dimensional nonlinear backward stochastic differential equations. *Discrete and Continuous Dynamical Systems - Series B (DCDS-B)*, 29(4):1695–1729, 2024.
- [33] Jan R. Magnus. The moments of products of quadratic forms in normal variables. *Statistica Neerlandica*, 32(4):201–210, 1978.
- [34] Peter E. Kloeden and Eckhard Platen. *Numerical Solution of Stochastic Differential Equations*. Springer, 1992.
- [35] Patrick Kidger, James Foster, Xuechen (Chen) Li, and Terry Lyons. Efficient and accurate gradients for neural sdes. In M. Ranzato, A. Beygelzimer, Y. Dauphin, P.S. Liang, and J. Wortman Vaughan, editors, *Advances in Neural Information Processing Systems*, volume 34, pages 18747–18761. Curran Associates, Inc., 2021.
- [36] Matthew Tancik, Pratul P. Srinivasan, Ben Mildenhall, Sara Fridovich-Keil, Nithin Raghavan, Utkarsh Singhal, Ravi Ramamoorthi, Jonathan T. Barron, and Ren Ng. Fourier features let networks learn high frequency functions in low dimensional domains. In *Proceedings of the 34th International Conference on Neural Information Processing Systems*, NIPS ’20, Red Hook, NY, USA, 2020. Curran Associates Inc.
- [37] James Bradbury, Roy Frostig, Peter Hawkins, Matthew James Johnson, Chris Leary, Dougal Maclaurin, George Necula, Adam Paszke, Jake VanderPlas, Skye Wanderman-Milne, and Qiao Zhang. JAX: composable transformations of Python+NumPy programs, 2018.
- [38] Christian Bender and Jianfeng Zhang. Time discretization and markovian iteration for coupled fbsdes. *The Annals of Applied Probability*, 18(1):143–177, 2008.
- [39] Zheyuan Hu, Zekun Shi, George Em Karniadakis, and Kenji Kawaguchi. Hutchinson trace estimation for high-dimensional and high-order physics-informed neural networks. *Computer Methods in Applied Mechanics and Engineering*, 424:116883, 2024.